JOURNAL OF APPLIED ELECTROCHEMISTRY 25 (1995) 592–602

Hydrogen evolution reaction on Ni–Al–Mo and Ni–Al electrodes prepared by low pressure plasma spraying

D. MIOUSSE, A. LASIA*

Département de Chimie, Université de Sherbrooke, Sherbrooke, Québec, Canada, J1K 2R1

V. BORCK

German Aerospace Research Establishment (DLR), Pfaffenwaldring 38-40, D-7000 Stuttgart 80, Germany

Received 3 June 1994; revised 4 November 1994

The hydrogen evolution reaction was studied on vacuum plasma sprayed Ni–Al and Ni–Al–Mo electrodes in 1 M NaOH and 25% KOH at 70 °C. It was found that Ni–Al–Mo electrode is more active in 25% KOH whereas Ni–Al electrode was more active in 1 M NaOH solutions. A.c. impedance measurements showed two semicircles on the complex plane plots. Two different equivalent models were used to explain this behaviour. The results indicate that the formation of the second semicircle is connected with the hydrogen evolution reaction.

1. Introduction

In the past decade many papers have dealt with ways of increasing the effectiveness of cathodes used for the hydrogen evolution reaction (HER) in alkaline solutions [1–4]. Nickel based electrodes are among the most active cathodes. Raney nickel type materials, which consist of the electrocatalytically active metal (Ni, Co, Cu) and a more active metal (Al, Zn), which can be easily leached out in alkaline solution, are characterized by a very large surface roughness [5–29]. Various techniques of preparation have been largely covered in the literature [1, 5–8, 12, 13]. For Ni–Al electrodes they include composite electrodeposition of the Raney nickel powder with nickel [6, 13, 17], plasma spraying [7, 11, 23, 24, 26], rolling of Ni–Al alloys [1, 11], interdiffusion of aluminium [14, 29] and sintering [5]. Ni–Zn electrodes were prepared by electrodeposition [15, 27] or by pressing nickel and zinc powders [28].

In our recent papers, Ni–Al electrodes were prepared by sintering Raney nickel at high pressure at 1400° C [5], heating Raney nickel with or without nickel powder at ~ 1700° C at which both metals melt [9], pressing Raney nickel and nickel powders [9] and by pressing and heating nickel and aluminium powders [29]. In the latter case it was found that a dramatic increase in activity occurs after heating Ni + Al powders above the aluminium melting point. Diffusion of aluminium into nickel and formation of Raney nickel is responsible for this high activity.

In the present paper, Ni–Al and Ni–Al–Mo alloys were prepared by low pressure plasma spraying [23–26]. This technique produced very active and stable electrode materials. The morphological changes on the surface were studied before and after the leaching process by scanning electron microscopy. The mechanism of the HER on these electrodes was studied by steady-state polarization and a.c. impedance techniques. Kinetic parameters and rate constants were extracted from the experimental results.

2. Theory

The hydrogen evolution reaction is known to proceed via three steps [5, 6, 27–32]. The first is the electroreduction of water with the formation of adsorbed hydrogen on the surface of the electrode (Volmer reaction). This is followed by an electrochemical (Heyrovsky reaction) or a chemical (Tafel reaction) desorption.

The faradaic reaction on a solid electrode can be usually represented by the equivalent circuit shown in Fig. 1(a) where the solution resistance, R_s, is in series with the parallel connection of a constant phase element (CPE) [35], and a faradaic impedance, Z_f. Harrington and Conway [32] described the faradaic admittance by

$$Y_f = \frac{1}{Z_f} = A + \frac{B}{j\omega + C} \quad (1)$$

where

$$A = \frac{1}{R_{ct}} = -F\left(\frac{\partial r_0}{\partial \eta}\right)_\Theta \quad (2)$$

$$B = -\frac{F^2}{\sigma_1}\left(\frac{\partial r_1}{\partial \eta}\right)_\Theta \left(\frac{\partial r_0}{\partial \Theta}\right)_\eta \quad (3)$$

$$C = -\frac{F}{\sigma_1}\left(\frac{\partial r_1}{\partial \Theta}\right)_\eta \quad (4)$$

$r_0 = \nu_1 + \nu_2$, $r_1 = \nu_1 - \nu_2 - 2\nu_3$, ν_1, ν_2 and ν_3 are the rates of the Volmer, Heyrovsky and Tafel reactions, respectively, η is the overpotential, Θ is the surface coverage by adsorbed hydrogen, and σ_1 is the charge

* To whom all correspondence should be addressed.

0021-891X

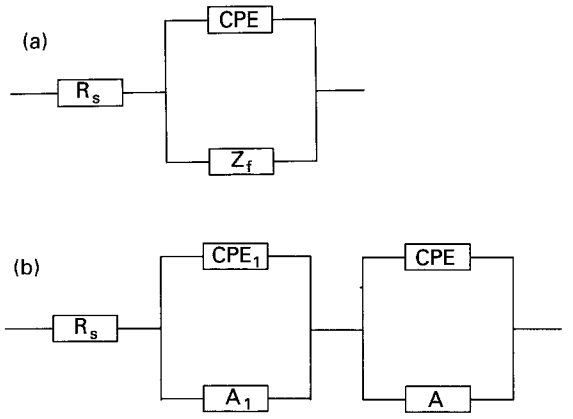

Fig. 1. Equivalent circuits for the HER: (a) CPE model; (b) two constant phase elements (CPE1–CPE) model.

necessary for the monolayer coverage by adsorbed hydrogen.

In general, this model predicts formation of two semicircles on the complex plane plots. These are intrinsically connected with the kinetics of the HER reaction. Such behaviour was observed on electrodes obtained by electrocodeposition of Raney nickel powder from a nickel bath [6, 17] and on a phosphate bonded rhodium on nickel powder electrode [33]. However, in most cases one semicircle was observed in past communications [16, 30, 34], which indicates that $A \gg B/(j\omega + C)$.

For solid electrodes the CPE element replaces the double layer capacitance. Its impedance is described by [5, 6, 9, 15–19, 27–30, 35]:

$$Z_{CPE} = \frac{1}{T(j\omega)^{\phi}} \tag{5}$$

where ϕ represents the rotation of the impedance semicircle on the complex plane plot and T is a parameter related to the average double layer capacitance, C_{dl} [35]:

$$T = C_{dl}^{\phi}(R_s^{-1} + A)^{1-\phi} \tag{6}$$

The surface roughness may also be taken into account in different ways in fractal [5, 9, 32, 36–42] and porous electrode models [43–46].

Another model leading to two semicircles in the complex plane contains a series connection of two parallel CPE–R circuits, Fig. 1(b). This model was developed to explain the a.c. impedance behaviour of Ni–Zn [28] and Ni–Al [29] powder electrodes. In this model the first semicircle was potential independent and its nature was attributed to the surface porosity [47], whereas the second one was connected with the HER. Theoretical simulations of the pear-shaped pores revealed the formation of a high frequency semicircle connected only with the surface porous structure.

The principal purpose of the present paper is to explain the nature of the two semicircles obtained for the HER on plasma sprayed electrodes and to determine the mechanism and kinetics of this reaction.

3. Experimental details

Ni–Al and Ni–Al–Mo electrodes were prepared by Borck from the German Aerospace Establishment using the low pressure plasma spraying technique [23, 24, 26]. Ni–Al alloy was deposited on both sides of perforated nickel sheets that were cut in pieces of 1 cm^2, giving a working surface of 2 cm^2. Ni–Al–Mo alloy was deposited on the upper surface of a copper cylinder (diameter 0.5 cm) and fitted in a shrinkable tube (Alpha Wire Corporation) giving a geometric area of 0.196 cm^2. Before the electrochemical tests, aluminium was leached out in a 25% KOH + 10% NaK-tartrate solution for 4 h at 70° C [24].

The microstructure of the electrode surface before and after leaching was studied by scanning electron microscopy (SEM). The electrochemical measurements were carried out in an H-type glass cell separated by a Nafion® membrane (DuPont de Neumours 324). The counter electrode was a nickel sheet (6 cm × 9 cm). A Luggin capillary was used to minimize the solution resistance. The uncompensated resistance was determined using the a.c. impedance method. The reference electrode was a Hg/HgO electrode in 1 M NaOH solution at room temperature. Electrochemical tests were made in 1 M NaOH (Aldrich semiconductor grade) and in 25% KOH solutions (Aldrich semiconductor grade) prepared using deionized water (Barnstead Nanopure). Tests were carried out at 70° C.

Equilibrium potentials of the hydrogen electrode were measured using a platinized platinum electrode [48] in the same electrolyte at the same temperature. The values obtained were −926 mV in the 25% KOH solution and −895 mV in the 1 M NaOH solution.

Before performing the a.c. impedance measurements, several Tafel curves were recorded until their variation could be neglected. Then, a constant current density of 250 mA cm^{-2} was applied for 30 min and a Tafel curve was recorded galvanostatically over the current range of 300 mA to 0.01 μA for the Ni–Al electrodes and 100 mA to 0.01 μA for the Ni–Al–Mo electrodes. The kinetic parameters (i.e., Tafel slope, b, exchange current density, j_o, and overpotential at the current density of 250 mA cm^{-2}, η_{250}) were obtained after correction for the uncompensated resistance, determined by a.c. impedance spectroscopy.

A.c. measurements were carried out using EG&G PAR system (Model 273) and a lock-in amplifier (Model 5208). Ten frequencies per decade were scanned from 10 kHz to 5 Hz using 5 mV peak-to-peak amplitude. Frequencies between 5 Hz and 0.01 Hz were scanned using a fast Fourier transform (FFT) technique. The approximation of the a.c. impedance spectra were performed using a modified complex nonlinear least-squares program [49]. All overpotentials reported were corrected for the uncompensated resistance.

4. Results

4.1. *Scanning electron microscopy*

SEM micrographs of the surface of the Ni–Al–Mo electrode are shown in Fig. 2. Significant differences

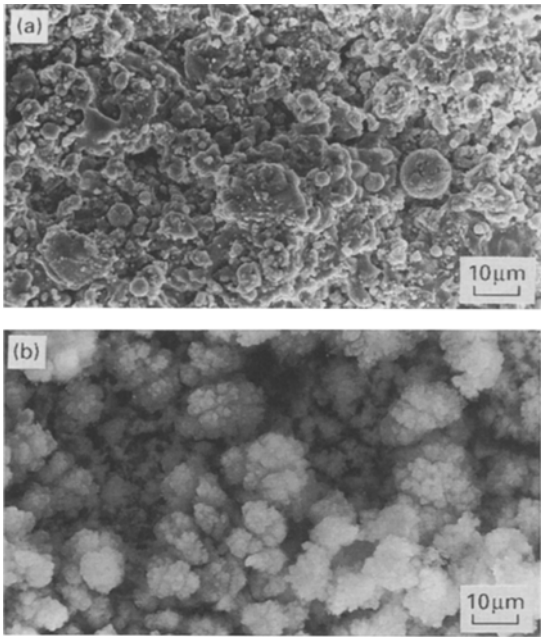

Fig. 2. Scanning electron micrographs of the Ni–Al–Mo electrodes: (a) before leaching; (b) after leaching aluminium in 25% KOH + 10% NaK tartrate solution at 70° C for 4 h.

in the electrode surface before and after leaching can be seen. Before leaching (Fig. 2(a)) the surface presents some spheres and other shapeless structures. After leaching (Fig. 2(b)) the surface presents a cauliflower like structure. A big increase in the porosity is also observed.

Figure 3 shows SEM micrographs of the Ni–Al electrode. The difference between the electrode surface before and after the leaching process is less significant than expected. Before leaching many small undefined structures can be seen but after leaching these have mostly disappeared.

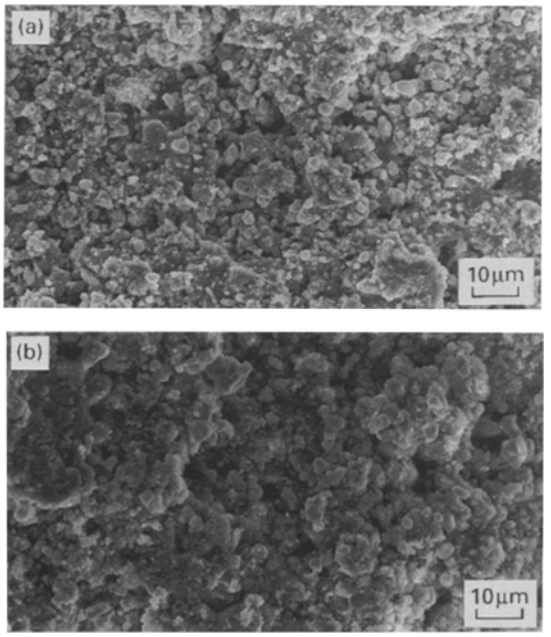

Fig. 3. Scanning electron micrographs of the Ni–Al electrodes: (a) before leaching; (b) after leaching aluminium in 25% KOH + 10% NaK tartrate solution at 70° C for 4 h.

4.2. *Ni–Al–Mo electrode*

4.2.1. Tafel curves. IR corrected polarization curves obtained on Ni–Al–Mo electrodes in 25% KOH and 1 M NaOH solutions at 70° C are shown in Fig. 4 and Table 1 presents corresponding kinetic parameters (j_o, b and η_{250}). A shift in the open circuit potential in the anodic direction was observed in 1 M NaOH. The electrode activity increases with increase in hydroxide concentration. The value of the hydrogen overpotential at 250 mA cm^{-2} in 25% KOH (74 mV) is half of that in 1 NaOH M (148 mV). Higher activity in more concentrated solution is also indicated by lower Tafel slope ~51 mV dec^{-1} and the higher current density, $j_0 \sim 9$ mA cm^{-2}.

4.2.2. A.c. impedance. The activity of the electrodes was also studied by the a.c. impedance technique. Two semicircles on the complex plane plots were obtained in both electrolytes at all overpotentials studied. The typical complex plane plots obtained for the Ni–Al–Mo electrodes are shown in Fig. 5.

It is interesting to note that the first semicircle is practically independent of the potential in both electrolytes whereas the second one decreases with increasing overpotential. This observation is similar to that observed on Ni–Zn [28] and Ni–Al [29] pressed powder electrodes.

To analyse a.c. impedance data, an electrical model has to be chosen. Two models shown in Fig. 1 approximated the experimental data well (both complex plane and Bode plots) and there were no statistical differences between them. To distinguish between these two models a detailed analysis of the results was carried out. In the model containing two CPE values corresponding to the first semicircle (CPE_1, A_1) are connected with the electrode porosity and those of the second one (CPE, A) are connected with the HER. In fact, Kreiser *et al.* [47] found the formation of a semicircle at high frequencies for pear shaped pores instead of a straight line observed for cylindrical pores. It should be added that using the fractal and porous electrode models it was impossible to approximate the impedance spectra well.

The dependence of the constant phase angle of the CPE element, Equation 5, on overpotential is presented in Fig. 6(a). It can be seen that the

Table 1. Kinetics parameters obtained from Tafel curves on Ni–Al–Mo and Ni–Al electrodes in 1 M NaOH and 25% KOH solutions at 70° C

Solution	*Slope*/mV dec^{-1}	j_0 /mA cm^{-2}	η_{250}/mV
(*Ni–Al–Mo*)			
1 M NaOH	71	2	148
25% KOH	51	9	74
(*Ni–Al*)			
1 M NaOH	59	4	105
25% KOH	84	9	119

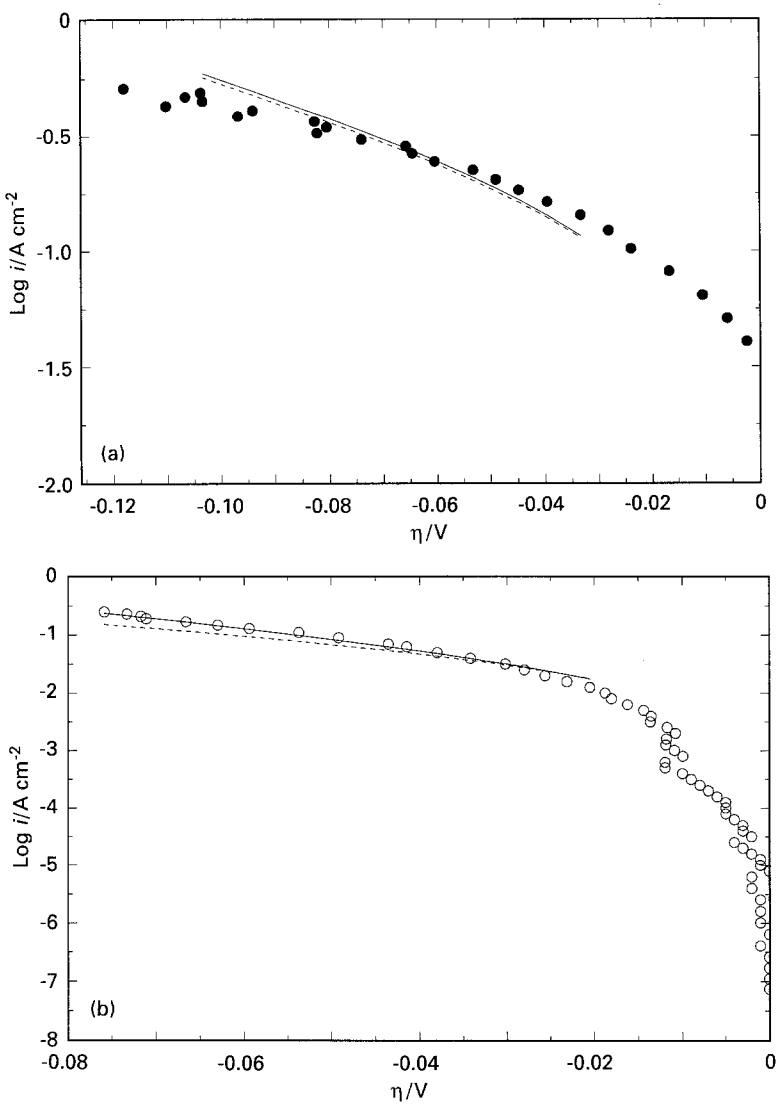

Fig. 4. Tafel curves obtained on Ni–Al–Mo electrodes at 70° C: (a) in 1 M NaOH; (b) in 25% KOH. Points are experimental, lines are obtained from the rate constants shown in Table 4 using the CPE model (solid line) and the CPE1–CPE model (dashed line).

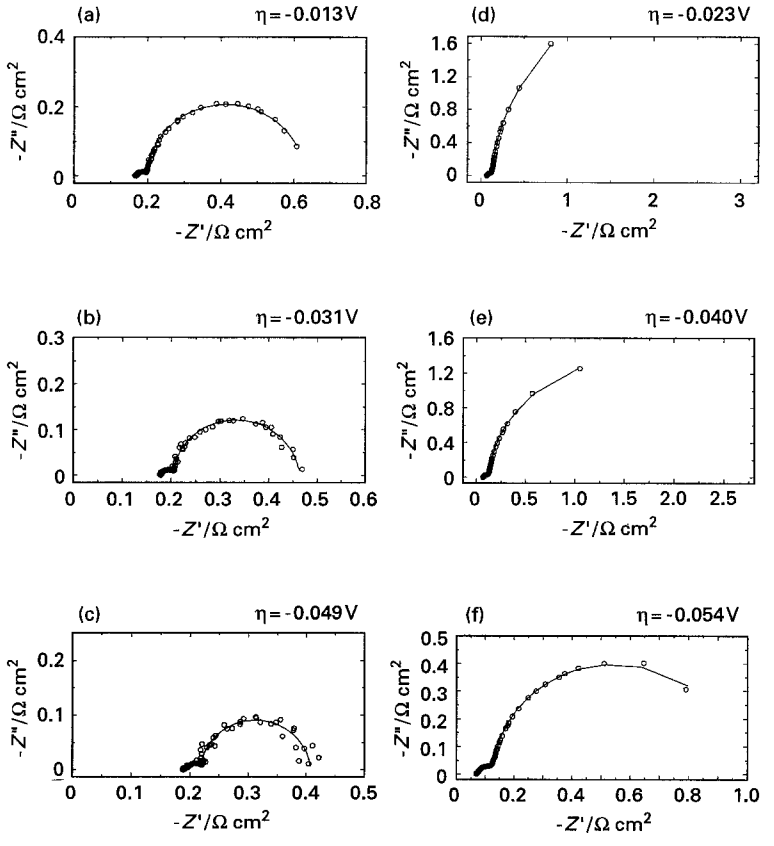

Fig. 5. Complex plane a.c. impedance spectra obtained on Ni–Al–Mo electrode in 1 M NaOH at 70° C (a–c) and in 25% KOH at 70° C (d–f).

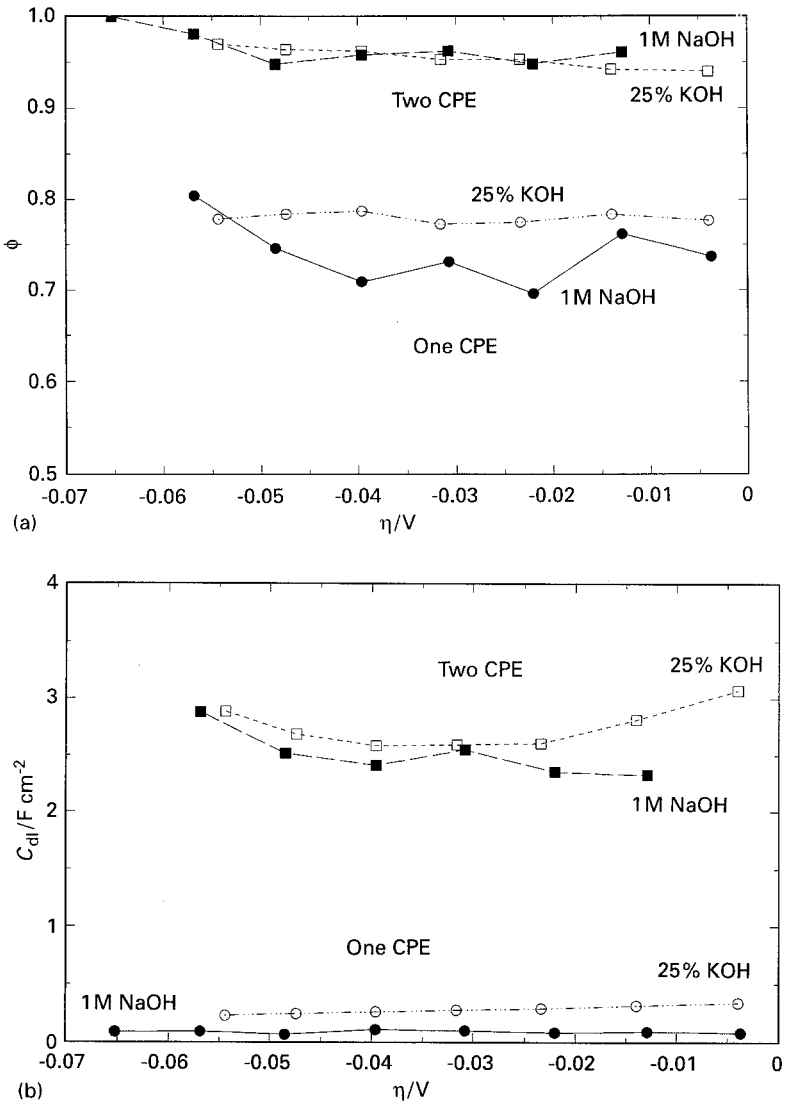

Fig. 6. Dependence of different parameters, Equation 6, on overpotential obtained for Ni–Al–Mo electrode at 70° C: (a) ϕ; (b) mean double layer capacitancies, C_{dl}. Filled symbols are obtained in 1 M NaOH solution and hollow ones in 25% KOH solution. Circles represent results obtained by the use of the CPE model and squares those obtained by the CPE1–CPE model.

parameter ϕ is approximately potential independent and equal to ~0.8 in 25% KOH and ~0.75 in 1 M NaOH assuming the one CPE model and ~0.95 using the two CPE model.

Using the values of T and phase angles the double layer capacitancies of the electrodes were calculated, Equation 6, and are shown in Fig. 6(b). The dependence of C_{dl} on overpotential has a similar shape as the dependence of T. Using the one CPE model, the electrode capacitance is larger in 25% KOH than in 1 M NaOH. In 1 M NaOH the values of C_{dl} are practically constant and equal ~0.09 F cm^{-2}. The values of C_{dl} obtained using the two CPE model are about 10 times larger in 25% KOH and 20 times larger in 1 M NaOH than the corresponding values obtained using the one CPE model.

Figure 7(a) shows the variation of $\log A$ on overpotential. The one CPE model indicates that the values of $\log A$ are practically potential independent in both solutions. The dependence of $\log A$ on overpotential is also different when the two CPE model is used. These values are lower than those obtained from the one CPE model. They also increase with increase in overpotential in both electrolytes.

For the one CPE model parameters B and C were determined. The dependence of parameters B and C on overpotential in both electrolytes is presented in Fig. 7(b) and (c). The values of B are negative and increase slightly with overpotential in both cases, they are also larger in 1 M NaOH than in 25% KOH. C values decrease slightly with overpotential and are smaller in 25% KOH than in 1 M NaOH. The values of parameters B and C are responsible for the appearance of the second semicircle which cannot be observed when $A \gg |B/C|$.

4.3. *Ni–Al*

4.3.1. Tafel curves. Figure 8 shows the polarization curves obtained at Ni–Al electrodes at 70° C. A shift of the open circuit potential in the positive direction is observed. A similar shift was also observed for Raney nickel electrodes [5, 9, 16, 34, 50, 51]. The kinetic parameters (b, j_0 and η_{250}) are displayed in Table 2. A decrease in activity with increase in alkali concentration was observed, in contrast to the behaviour of Ni–Al–Mo electrodes. A similar decrease in activity was also observed for other Raney nickel electrodes [6, 17–19, 50].

The Ni–Al electrode shows a higher activity than the Ni–Al–Mo electrode in 1 M NaOH; however, the opposite was observed in 25% KOH. The two

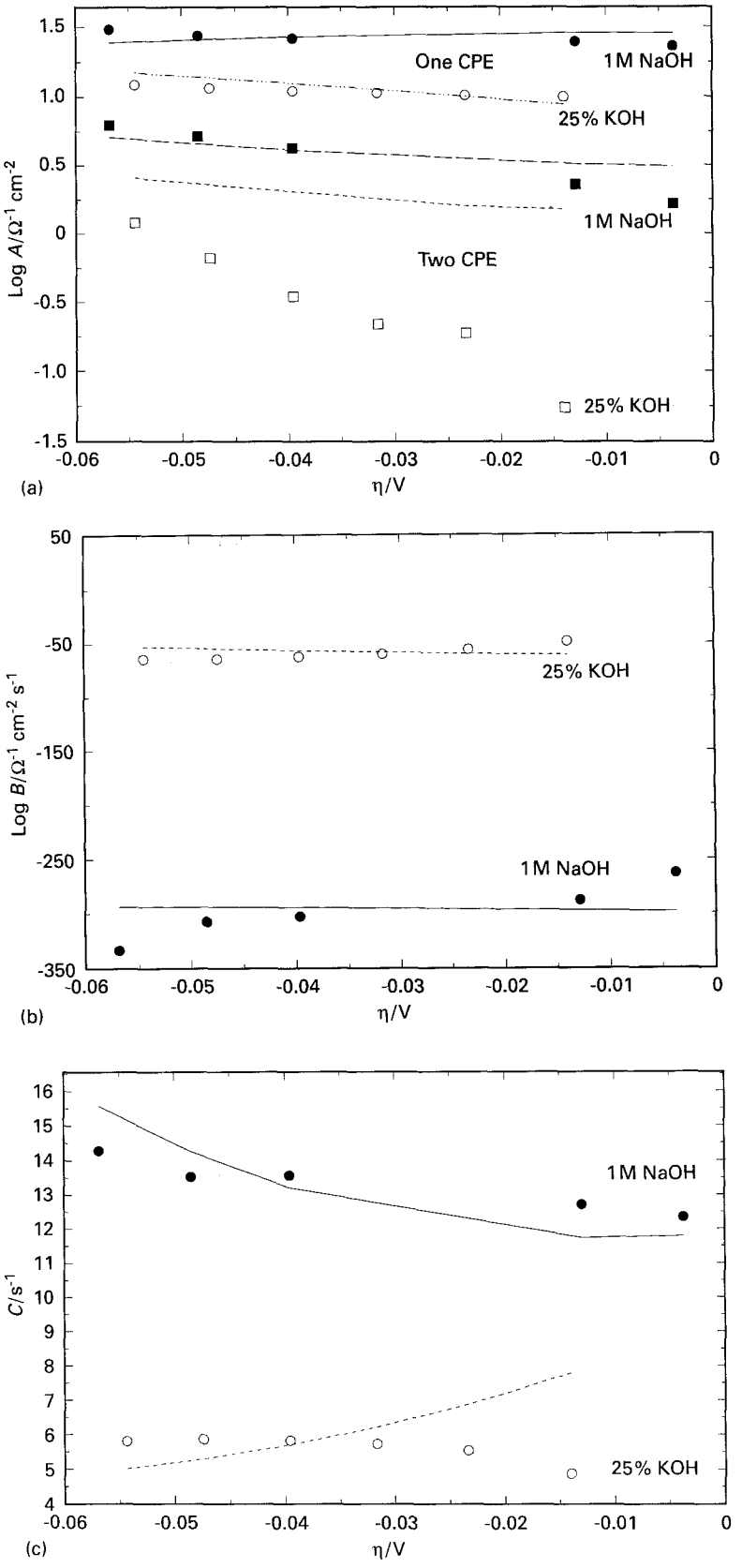

Fig. 7. Dependence of parameters A, B and C, Equations 1–4, on overpotential for Ni–Al–Mo electrode at 70° C: (a) $A(=1/R_{ct})$; (b) B; (c) C. Filled symbols correspond to data obtained in 1 M NaOH solution and hollow to 25% KOH solution. Circles represent results obtained by the use of the CPE model and squares those obtained by the CPE1–CPE model. Lines are calculated using rate constants shown in Table 3.

electrodes are more active than Ni–Zn [28] and Ni–Mo [34] powder electrodes and Ni–Zn alloy [15] electrodes. Their activity is lower than that of Ni–Al powders heated at 700° C [29].

4.3.2. A.c. impedance. Typical complex plane plots are shown in Fig. 9. In both electrolytes, two semicircles were observed and the first one varied with overpotential. This behaviour is different from that described above where the first semicircle was potential independent. As above, two models (Fig. 1) were used to explain the a.c. impedance behaviour. Similarly to the previous case there were no statistically significant differences between the approximations obtained using these two models.

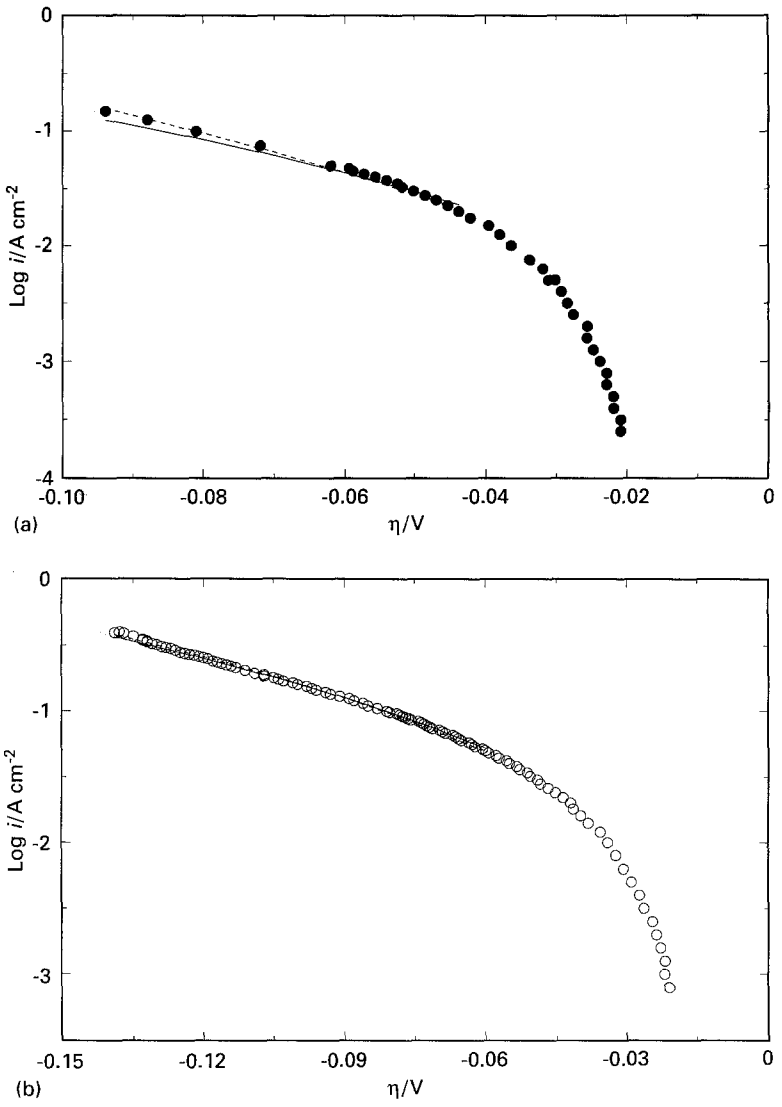

Fig. 8. Tafel curves obtained on Ni–Al electrodes at 70° C: (a) in 1 M NaOH; (b) in 25% KOH. Points are experimental, lines are obtained from the rate constants shown in Table 3 using the CPE model (solid line) and the CPE1–CPE model (dashed line).

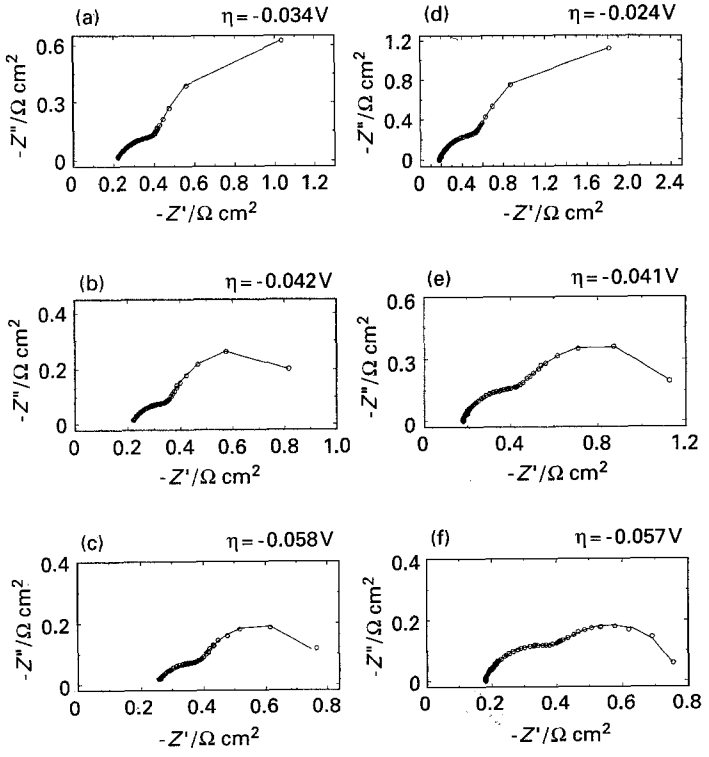

Fig. 9. Complex plane a.c. impedance spectra obtained on Ni–Al electrode in 1 M NaOH at 70° C (a–c) and in 25% KOH at 70° C (e–f).

Table 2. Kinetic parameters obtained from a.c. impedance and steady-state polarization measurements for Ni–Al–Mo and Ni–Al electrodes at 70 °C

Solution	k_1/mol cm^{-2} s^{-1}	k_{-1}/mol cm^{-2} s^{-1}	k_2/mol cm^{-2} s^{-1}
(Ni–Al)			
1 M NaOH	$2.3 \pm 0.7 \times 10^{-7}$	$2.0 \pm 0.4 \times 10^{-8}$	$9 \pm 1 \times 10^{-7}$
25% KOH	$2.8 \pm 0.2 \times 10^{-7}$	$2.6 \pm 0.3 \times 10^{-8}$	$5.4 \pm 0.4 \times 10^{-7}$
(Ni–Al–Mo)			
1 M NaOH	$5.8 \pm 0.3 \times 10^{-7}$	$4.1 \pm 0.5 \times 10^{-7}$	$1.4 \pm 0.2 \times 10^{-5}$
25% KOH	$1.1 \pm 0.4 \times 10^{-6}$	$4.8 \pm 0.4 \times 10^{-8}$	$2.3 \pm 0.2 \times 10^{-6}$

Figure 10a shows the dependence of the constant phase angle on overpotential. In terms of the one CPE model mean values of ϕ are similar in both electrolytes and equal to ~0.8. For the two CPE model these values decrease from ~1 to ~0.85 with increasing negative overpotential.

The dependence of C_{dl} is shown in Fig. 10(b). The variation of C_{dl} follows that of the parameter T. Their values are practically independent of overpotential and are larger in 1 M NaOH, in contrast to the results obtained on Ni–Al–Mo electrodes. The values of the C_{dl} are 10 to 15 times larger when the two CPE model is used.

Figure 11(a) shows the dependence of $\log A$ on overpotential, $\log A$ increases with increase in negative overpotential. On the basis of the one CPE model the values of $\log A$ are smaller in 25% KOH than in 1 M NaOH, in agreement with the results of steady-state polarization experiments, Table 1. At large overpotentials values of $\log A$ obtained by the two models are similar; however, larger differences are observed at lower overpotentials.

The dependence of the parameters B and C on overpotential is presented in Fig. 11(b) and (c). Parameter B is negative and $|B|$ and C increase with increase in negative overpotential. Values of the parameter $|B|$ are much smaller (~100 times) than those for the Ni–Al–Mo electrode. It can be observed that the second semicircle on the complex plane plots is smaller for the Ni–Al electrode (Fig. 9) than for the Ni–Al–Mo electrode (Fig. 5). The values of C increase with increase in negative overpotential for two solutions. The values of parameter C are ~5–15 times smaller than those for the Ni–Al–Mo electrode.

4.4. *Rate constants and intrinsic activities*

The rate constants for the HER on both electrodes were obtained by the NLS approximation of the experimental results [5, 6, 9, 15–17, 27–30, 33, 34]

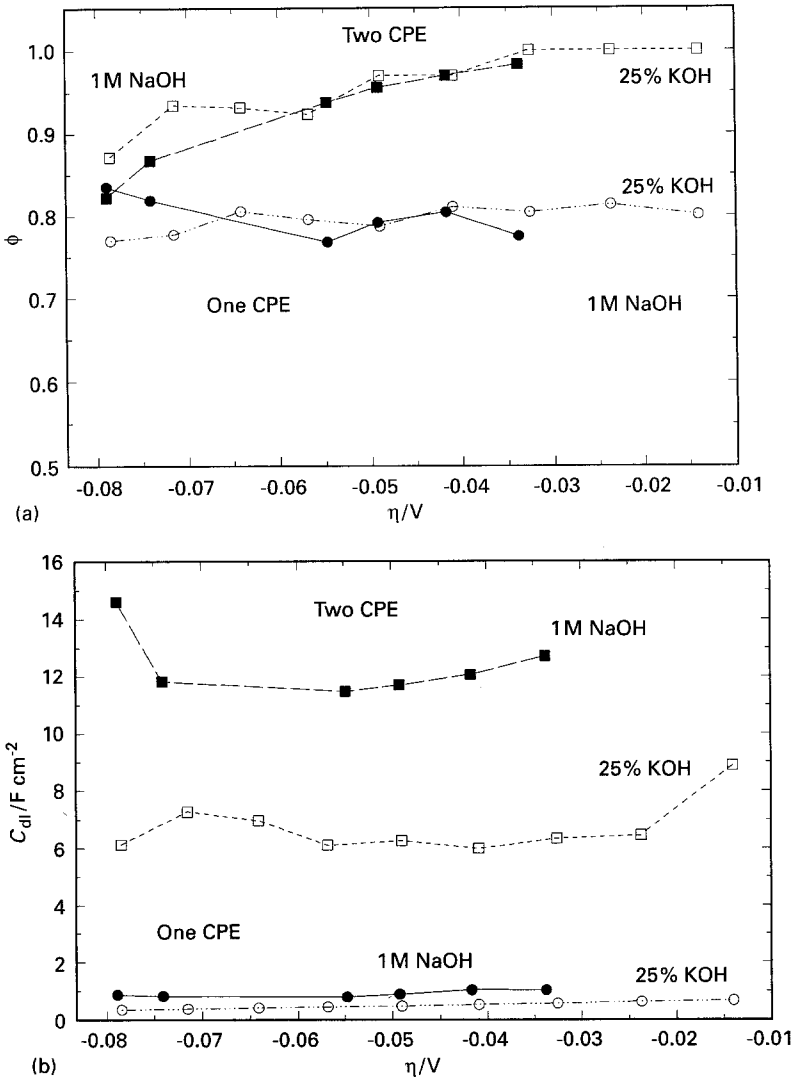

Fig. 10. Dependence of different parameters, Equation 6, on overpotential obtained for Ni–Al electrode at 70° C: (a) ϕ; (b) mean double layer capacitancies, C_{dl}. Filled symbols are obtained in 1 M NaOH solution and hollow ones in 25% KOH solution. Circles represent results obtained by the use of the CPE model and squares those obtained by the CPE1–CPE model.

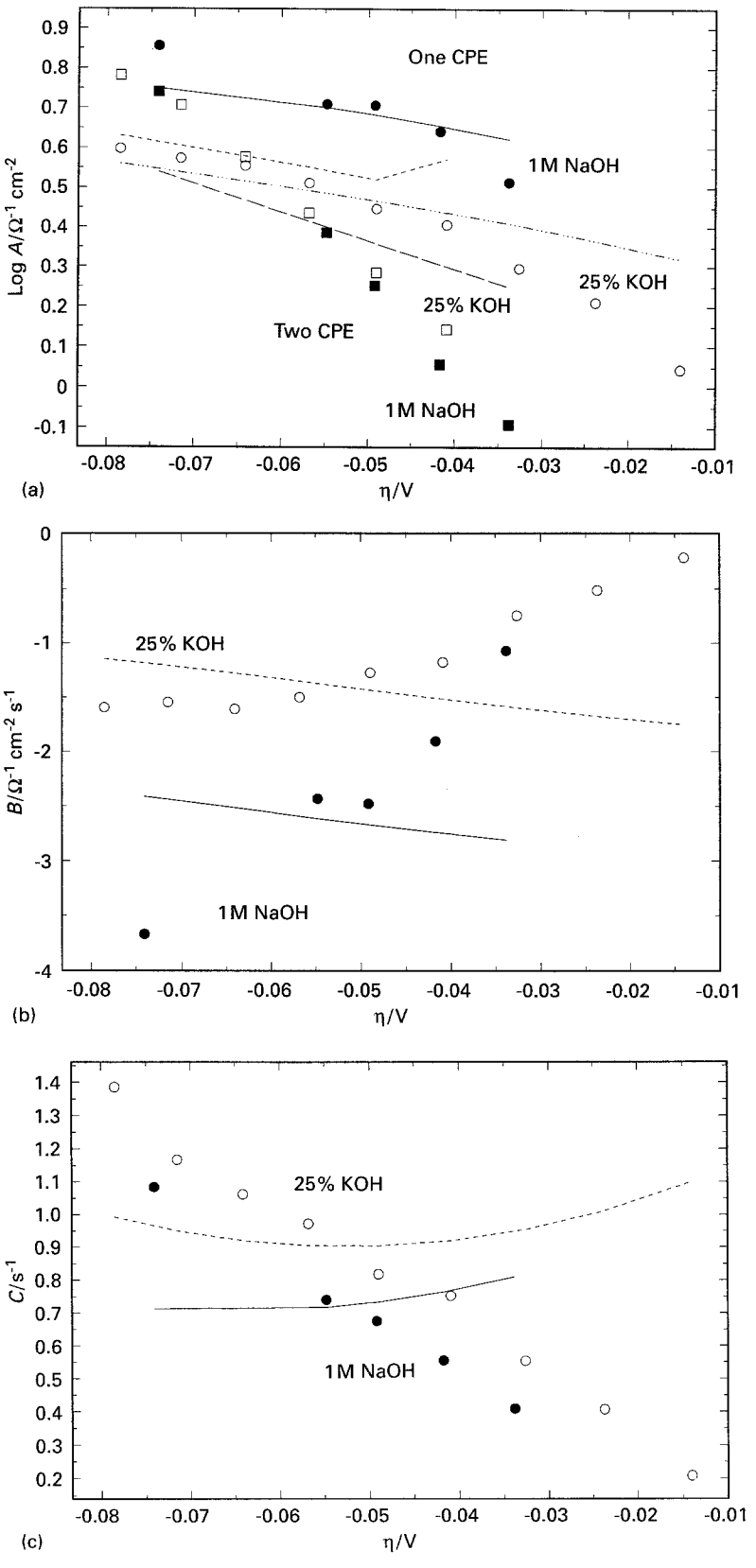

Fig. 11. Dependence of parameters, Equations 1–4 on overpotential obtained for Ni–Al electrode at 70° C: (a) A $(= 1/R_{ct})$; (b) B; (c) C. Filled symbols are obtained in 1 M NaOH solution and hollow ones in 25% KOH solution. Circles represent results obtained by the use of the CPE model and squares those obtained by the CPE1–CPE model. Lines are calculated using rate constants shown in Table 2.

assuming the Volmer–Heyrovsky mechanism. Two sets of data, obtained using two electrical equivalent models, were used.

For the one CPE model, values of A, B, C and i were used in order to determine the rate constants and the values are shown in Table 2. Simulated curves are presented in Figs 4 and 7 in the case of the Ni–Al–Mo electrodes and in Figs 8 and 11 for the Ni–Al electrodes.

For the two CPE model, values of the parameter A of the second semicircle and currents i were used in order to determine the rate constants. Best simulated curves obtained are presented in Figs 4 and 7 for the Ni–Al–Mo electrodes and in Figs 8 and 11 for the Ni–Al electrodes. It can be seen that the approximation is good for the Tafel curves. Approximation of the a.c. impedance parameters for the Ni–Al electrode are, in general,

Table 3. Comparison of the roughness factor, R, and the real rate constant, k_1/R, for different electrodes at 70 °C

Electrode	*Condition*	*R*	k_1/R mol cm^{-2} s^{-1}	*Reference*
Ni–Al	1 M NaOH	45 000	5.1×10^{-12}	this work
	25% KOH	25 000	1.1×10^{-11}	
Ni–Al–Mo	1 M NaOH	4000	1.5×10^{-10}	this work
	25% KOH	14 000	7.9×10^{-11}	
Ni–Al powders heated at 700 °C	1 M NaOH	60 000	7.0×10^{-12}	29
Raney Ni + Ni powders	1 M NaOH	10 000	2.5×10^{-11}	9
Amorphous Ni_2B	1 M NaOH	14 000	9.0×10^{-12}	16
Amorphous Ni_2B + Ni	1 M NaOH	48 000	5.0×10^{-12}	16
Electrodeposited Raney Ni + Ni	1 M NaOH	3500	6.6×10^{-11}	6

much worse than those found for the Ni–Al–Mo electrode.

These results indicate that the one CPE model is more probable because it agrees better with the experimental data. It should be added that this model was also used for electrocodeposited Raney nickel electrodes [6].

The surface roughness of the Ni–Al–Mo electrode is generally smaller than that of the Ni–Al electrode. Moreover, change in the roughness with increase in the alkali concentration is different for these two electrodes. For Ni–Al it decreases and for Ni–Al–Mo it increases with increase in the electrolyte concentration. The change in the surface roughness factor is in agreement with the change in the electrochemical activity (Table 1), the activity of the Ni–Al–Mo electrode increases and that of Ni–Al decreases with increase in the alkali concentration. The behaviour observed for plasma sprayed Ni–Al electrode is similar to that found for electrocodeposited Raney nickel electrodes [6, 17–19, 50].

Table 3 shows the values of the intrinsic (divided by the surface roughness) rate constants of the slowest step. It indicates that the intrinsic activity of Ni–Al–Mo electrode is larger than that of Ni–Al, although determination of the geometrical surface area of the Ni–Al electrode was more difficult because it was deposited on a grid.

5. Conclusions

Studies of the electrochemical activities of vacuum plasma sprayed Ni–Al–Mo and Ni–Al electrodes were performed using steady-state polarization and a.c. impedance methods. Two equivalent electrical circuits shown in Fig. 1 were used. It was found that the Ni–Al–Mo electrode is more active in 25% KOH although the opposite is observed in 1 M NaOH. It has been found earlier [24] that this electrode is more stable in long time studies. The approximations of the electrochemical measurements indicated that the one CPE model is more probable, that is the second semicircle is connected with *B* and *C* parameters. Although the surface roughness of the Ni–Al electrode is larger (45 000 and 25 000 in 1 M NaOH and 25% KOH, respectively) than that of Ni–Al–Mo electrode (4000 and 14 000, respectively) the activity of the latter is higher. This indicates higher intrinsic activity of this electrode, Table 3, especially in 1 M NaOH. This is the first example of a significant increase in the intrinsic catalytic activity of nickel based electrodes [46, 52]. Up to now, known nickel based electrodes had similar intrinsic activities. The roughness of the Ni–Al electrode is similar to that composed of 90% of amorphous Ni_2B + 10% Ni powders [16] and larger than that of Raney Ni + Ni pressed powders [9] or electrocodeposited Raney Ni + Ni [6]. However, it is smaller than that of Ni + Al powder electrode heated above the aluminium melting point [29], where Raney nickel is formed *in situ*. However, the kinetic parameters determined for this electrode are much less precise because of the larger error in the determination of the geometrical surface area; the Ni–Al electrode was deposited on a nickel grid whereas Ni–Al–Mo electrode was deposited on a copper cylinder. It should be noticed that the adherence of the deposit to copper base was much weaker than that to the metallic grid. The presence of molybdenum in the alloy changes the structure of the deposit, the grains are smaller and a significant enrichment of the Ni_2Al_3 phase was observed [53]. The presence of pure molybdenum islands was also found. This structure apparently increases the electrode activity and stability. The increase in activity of nickel after introduction of molybdenum was also observed in the literature [11], however, the electrodeposited Ni–Mo alloy was found to be more active than the plasma sprayed coatings.

Another interesting observation is a large increase in the surface roughness of the Ni–Al–Mo electrode when going from 1 M NaOH to 25% KOH, whereas the activity of vacuum plasma sprayed Ni–Al electrode decreased. The behaviour or the Ni–Al–Mo electrode is different from that found for Raney nickel [6, 17–19, 50].

The results indicate that the structure and surface of the Ni–Al–Mo electrode obtained after leaching out aluminium is responsible for the high activity. It is also interesting to note that despite increase in the solution concentration when changing from 1 M NaOH to 25% KOH the accessibility of the surface increases.

Acknowledgements

Financial support from NSERC and FCAR (grant for D.M.) is gratefully acknowledged.

References

[1] D. Ohms, V. Plzak, S. Trasatti, K. Wiesener and H. Wendt, *in* 'Electrochemical hydrogen technologies. Electrochemical production and combustion of hydrogen', (edited by H. Wendt), Elsevier, New York (1990) p. 1.
[2] S. Trasatti, *in* 'Advances in electrochemical science and engineering', vol. 2 (edited by H. Gerisher and C. W. Tobias), VCH, Weinheim, (1992) pp. 1–85.
[3] J. Divisek, H. Schmitz and J. Balej, *J. Appl. Electrochem.* **19** (1989) 519.
[4] M. Enyo, *in* 'Comprehensive treatise of electrochemistry', vol. 7 (edited by B. E. Conway, J. O'M. Bockris, E. Yeager, S. U. M. Khan and R. E. White), Plenum Press, New York (1983) p. 241.
[5] A. Rami and A. Lasia, *J. Appl. Electrochem.* **22** (1992) 376.
[6] Y. Choquette, L. Brossard, A. Lasia and H. Ménard, *J. Electrochem. Soc.* **137** (1990) 1723.
[7] D. E. Hall, *J. Appl. Electrochem.* **14** (1984) 107.
[8] *Idem, J. Electrochem. Soc.* **128** (1981) 740.
[9] P. Los, A. Rami and A. Lasia, *J. Appl. Electrochem.* **23** (1993) 135.
[10] J. P. Diard, B. Legorrec and S. Maximovitch, *Electrochim. Acta* **35** (1990) 1099.
[11] B. V. Tilak, A. C. Ramamurthy and B. E. Conway, *Proc. Indian Acad. Sci. (Chem. Sci.)* **97** (1986) 359.
[12] I. A. Raj and K. I. Vasu, *J. Appl. Electrochem.* **20** (1990) 32.
[13] E. Endoh, H. Otouma, T. Morimoto and Y. Oda, *Int. J. Hydrogen Energy* **12** (1987) 473.
[14] C. R. S. Needs and N. Del, *US Patent 4 116 804* (1978).
[15] L. Chen and A. Lasia, *J. Electrochem. Soc.* **139** (1992) 1058.
[16] P. Los and A. Lasia, *J. Electroanal. Chem.* **333** (1992) 115.
[17] Y. Choquette, L. Brossard, A. Lasia and H. Ménard, *Electrochim. Acta* **35** (1990) 1251.
[18] Y. Choquette, H. Ménard and L. Brossard, *Int. J. Hydrogen Energy* **14** (1989) 637.
[19] Y. Choquette, H. Ménard and L. Brossard, *ibid.* **15** (1990) 21.
[20] M. J. De Giz, J. C. P. Silva, M. Ferreira, S. A. S. Machado, E. A. Ticianelli, L. A. Avaca and E. R. Gonzalez, *ibid.* **17** (1992) 725.
[21] M. J. De Giz, S. A. S. Machado, L. A. Avaca and E. R. Gonzalez, *J. Appl. Electrochem.* **22** (1992) 973.
[22] J. Divisek, P. Malinowski, J. Mergel and H. Schmitz, *Int. J. Hydrogen Energy* **13** (1988) 141.
[23] A. Kayser, V. Borck, M. von Bradke, R. Henne, W. A. Kaysser and G. Schiller, *Z. Metallkd.* **83** (1992) 7.
[24] G. Schiller and V. Borck, *Int. J. Hydrogen Energy* **17** (1992) 261.
[25] S. Rausch and H. Wendt, *J. Appl. Electrochem.* **22** (1992) 1025.
[26] R. Henne, W. Schnurnberger and W. Weber, *Thin Solid Films* **119** (1984) 141.
[27] L. Chen and A. Lasia, *J. Electrochem. Soc.* **138** (1991) 3321.
[28] L. Chen and A. Lasia, *ibid.* **139** (1992) 3214.
[29] *Idem, ibid.* **140** (1993) 2721.
[30] A. Lasia and A. Rami, *J. Electroanal. Chem.* **294** (1990) 123.
[31] L. Bai, D. A. Harrington and B. E. Conway, *Electrochim. Acta* **32** (1987) 1713.
[32] D. A. Harrington and B. E. Conway, *ibid.* **32** (1987) 1703.
[33] P. K. Wrona, A. Lasia, M. Lessard and H. Ménard, *ibid.* **37** (1992) 1283.
[34] H. Dumont, P. Los, L. Brossard, A. Lasia and H. Ménard, *J. Electrochem. Soc.* **139** (1992) 2143.
[35] G. B. Brug, A. L. G. van den Eeden, M. Sluyters-Rehbach and J. H. Sluyters, *J. Electroanal. Chem.* **176** (1984) 275.
[36] L. Chen and A. Lasia, *J. Electrochem. Soc.* **139** (1992) 3458.
[37] R. de Levie, *J. Electroanal. Chem.* **281** (1990) 1.
[38] *Idem, ibid.* **261** (1989) 1.
[39] *Idem, Electrochim. Acta* **9** (1964) 1231.
[40] *Idem, ibid.* **10** (1965) 395.
[41] L. Nyikos and T. Pajkossy, *ibid.* **30** (1985) 1533.
[42] T. Pajkossy and L. Nyikos, *J. Electrochem. Soc.* **133** (1986) 2086.
[43] J.-P. Candy and P. Fouilloux, *Electrochim. Acta* **26** (1981) 1029; *ibid.* **27** (1982) 1585.
[44] L. M. Gassa, J. R. Vilche, M. Ebert, K. Juttner and W. J. Lorenz, *J. Appl. Electrochem.* **20** (1990) 677.
[45] R. de Levie, *Adv. Electrochem. Electrochem. Eng.* **6** (1967) 329.
[46] A. Lasia, *Int. J. Hydrogen Energy* **18** (1993) 557.
[47] H. Kreiser, K. D. Beccu and M. A. Gutjahr, *Electrochim. Acta* **21** (1976) 539.
[48] G. J. Hills and D. J. G. Ives, *J. Chem. Soc.* (1951) 305.
[49] J. R. Macdonald, J. Schoonman and A. P. Lehner, *J. Electroanal. Chem.* **131** (1982) 77.
[50] E. Potvin, H. Ménard, J. M. Lalancette and L. Brossard, *J. Appl. Electrochem.* **20** (1990) 252.
[51] E. Potvin, A. Lasia, H. Ménard and L. Brossard, *J. Electrochem. Soc.* **138** (1991) 900.
[52] A. Lasia, *in* 'Current topics in electrochemistry, research trends', in press.
[53] R. Henne, A. Kayser, V. Borck and G. Schiller, Proceedings of the International Thermal Spray Conference, Orlando, FL, (1992) p. 817.